PHOTOMASK

BACUS—The international technical group of SPIE dedicated to the advancement of photomask technology.

# Improved Ru/Si multilayer reflective coatings for advanced extreme ultraviolet lithography photomasks

**Obert Wood, Keith Wong, Valentin Parks, Mohammad Faheem, Yifan Liang, Ajay Kumar, Esther Chen, Corbin Bennett, Bianzhu Fu, Michael Gribelyuk, Wayne Zhao, Pawitter Mangat, and Paul van der Heide,** GLOBALFOUNDRIES, 400 Stonebreak Rd. Extension, Malta, NY 12020 USA

**Patrick Kearney,** SUNY Poly SEMATECH, 257 Fuller Road, Albany, NY 12203 USA

**Julia Meyer-Ilse,** Lawrence Berkeley National Laboratory, 1 Cyclotron Road, Berkeley, CA 94720 USA

**Vu Luong and Vicky Philipsen,** IMEC, Kapeldreef 75, B-3001 Leuven, Belgium

## ABSTRACT

Extreme ultraviolet (EUV) lithography with reflective photomasks continues to be a potential patterning technology for high volume manufacturing at the 7 nm technology node and beyond. EUV photomasks with alternative materials to the commonly used Mo/Si multilayer (ML) reflector and patterned Ta-based absorber (both of which are known to require shadow effect corrections and lead to large through-focus pattern placement errors) are being actively explored. Because the reflective bandwidth of a Ru/Si ML is significantly wider than the reflective bandwidth of a Mo/Si ML and the effective reflectance plane in Ru/Si is closer to the ML surface, Ru/Si ML coatings may be viable alternatives to the Mo/Si ML coatings that are commercially available today because they will lead to smaller mask 3D effects. In this paper, increases in the peak reflectivity and the reflective bandwidth of Ru/Si ML reflectors by using $B_4C$ interlayers to improve the Ru-Si interfaces are discussed. The conclusions of this paper are supported with the results of both experimental measurements and rigorous simulations.

## 1. Introduction

All extreme ultraviolet masks are comprised of a multilayer film stack, which ideally provides a high reflectivity for all occurring angles of incidence, and a patterned absorber or shifter layer, which

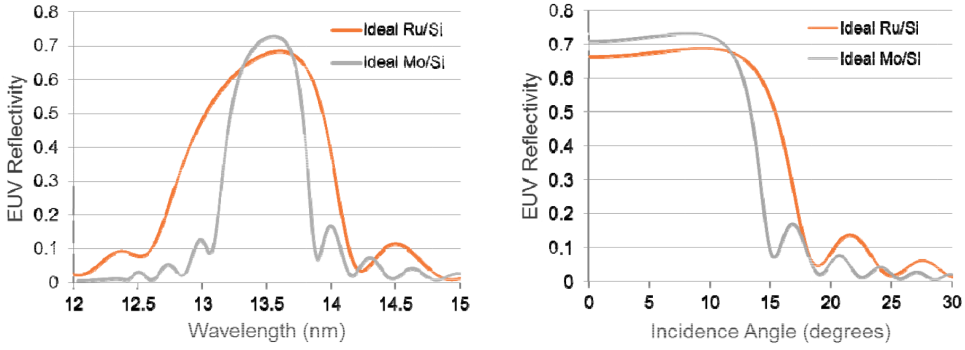


*Figure 1. Left: Plots of reflectivity versus EUV wavelength at 6° angle of incidence for an ideal Mo/Si ML with 40 bilayers (in grey) and an ideal Ru/Si ML with 20 bilayers (in red). Right: Plots of EUV reflectivity versus incident angle at 13.5 nm wavelength for an ideal Mo/Si ML with 40 bilayers (in grey) and an ideal Ru/Si ML with 20 bilayers (in red).*

BACUS NEWS

JUNE 2016
VOLUME 32, ISSUE 6

TAKE A LOOK INSIDE:



SPIE.

AL16 9776-46

# EDITORIAL

## No Rest for the Mask Industry

**By Moshe Preil and Mark Wylie,** KLA-Tencor

The past several years in the mask making industry have seen a slight deceleration in the rate of technical progress and shrinking geometries. With 193 nm immersion reaching the limits of single patterning several nodes ago, the recent node shrinks have been driven by multiple patterning processes. Devices on the wafer have continued to shrink, but the primary features at the mask level and the amount of data written to a single mask leveled off. Instead, multiple masks with tighter registration tolerances are now needed to print a single level at the wafer, and more attention has been directed towards edge placement error (EPE) rather than separate specifications for CD and overlay.

Unlike the "mask maker's holiday" of the 1980s to early 1990s when 1x masks were replaced by 4x and 5x reticles, this recent relaxation in the rate of shrinking geometries and tighter specs has been more of a working vacation. Most mask makers would argue it was barely a long weekend, and like any time off in the internet era, we had to take our computers with us and stay connected at all times.

We are now entering an era with many exciting challenges to tackle after the recent short pause. EUV is once again picking up momentum with stronger forecasts for adoption. This sustained momentum will drive the mask industry to solve many new challenges associated with the transition from research to high volume manufacturing (HVM). While perfect defect free mask blanks will still not be available in steady volumes, blank quality will be driven to meet the defect requirements by finding all of the pits, bumps and embedded multi-layer defects that could create phase defects up stream in the mask patterning process. Mapping the exact locations of these known defects will allow pattern shifting to be utilized to cover the known defect locations, thereby allowing the final patterned mask inspection to be carried out without actinic EUV inspection.

Line edge roughness (LER) and placement error from the pattern generation steps will need to be improved to ensure the mask component is not consuming all of the LER and EPE budgets. More of these critical budgets will need to be allocated to the wafer side to deal with the limitations of shot noise and resist sensitivity available today for the wafer exposure system (though there are still emerging advances in this area). For the mask maker there are slow activation resists which can greatly reduce LER, however these create a number of challenges with the current pattern generation technologies. These challenges require either higher dose, which can lead to increased defect rates, or multiple passes, which could mean multiple days of exposure on current generation e-Beam tools and is not economically viable.

There are other key challenges with EUV mask adoption associated with the available pellicle technologies. One path receiving strong support is the use of a removable pellicle developed by ASML which can be mounted and demounted without the use of any adhesives, thereby solving the outgassing and contamination issues and enabling rapid replacement in case of pellicle failures over time. The current membrane is opaque to DUV laser's utilized on the current generation of mask inspection tools, but a clean removal and remounting process should enable the continued use of these tools. There are other pellicle options which could be inspected with the pellicle in place such as those proposed by IBM at the recent SPIE Symposium on Advanced Lithography 2016 (AL16) as well as technical feasibility studies at IMEC. All of these options must still overcome a number of challenges such as thermal stress imposed by the reaction to EUV light, longevity of the pellicle due to the reduced transmission rates and the economical scale up of the new pellicle industry to support HVM. The final decisions on the pellicle technologies and architectures will then define what can be done for through pellicle inspection and determine whether a DUV inspection tool can still be used, thereby enabling an ideal cost effective and available solution for the industry.

On the mask writing side, recently reported advances in multi-beam exposure technologies would lead to economically viable solutions to improve EUV mask pattern generation, enabling improved pattern fidelity and reduced LER. This new e-Beam technology can also be utilized to enable more aggressive optical proximity correction (OPC) techniques for optical mask technologies which could help enable more process latitude for today's 193 immersion scanners and potentially helping to reduce the number of lithographic weak

*(continued on page 9)*

BACUS

N • E • W • S

*BACUS News* is published monthly by SPIE for BACUS, the international technical group of SPIE dedicated to the advancement of photomask technology.

**Managing Editor/Graphics** Linda DeLano
**Advertising** Melissa Farlow
**BACUS Technical Group Manager** Pat Wight



SPIE.

P.O. Box 10, Bellingham, WA 98227-0010 USA
Tel: +1 360 676 3290
Fax: +1 360 647 1445
www.SPIE.org
help@spie.org

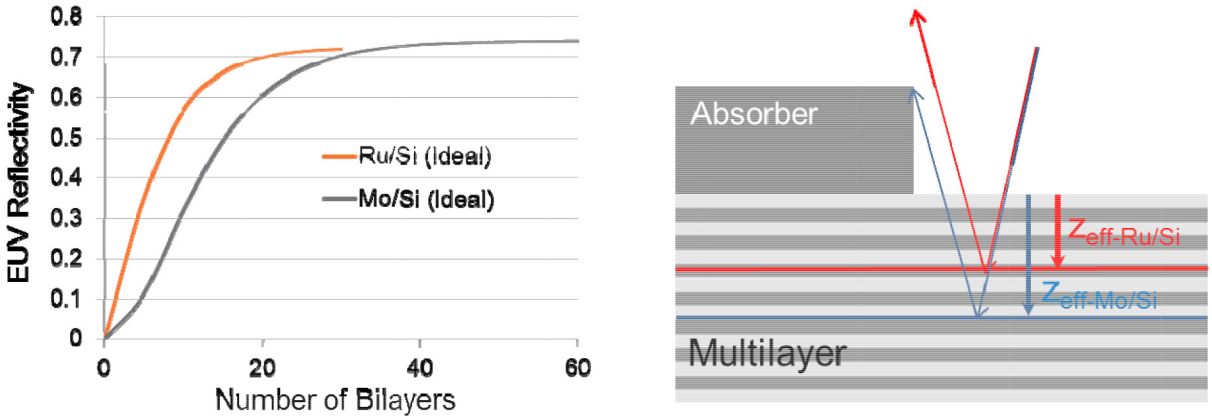


*Figure 2. Left: Plots of reflectivity at 13.5 nm wavelength and 6° angle of incidence versus the number of bilayers for an ideal Ru/Si ML (in red) and an ideal Mo/Si ML (in grey). Right: Cross section of an EUV mask stack illustrating the relative position of the effective reflectance plane ($Z_{eff}$) in Ru/Si and Mo/Si ML coatings: $Z_{eff}$ ~ 33 nm in Ru/Si and $Z_{eff}$ ~ 45 nm in Mo/Si. Note: multilayer period shown schematically is not to scale.*

defines the features on the mask. Because EUV reflective masks are illuminated at an oblique angle in order to separate incident and reflected light, their coating structure has an inordinately large impact on image quality and gives rise to a horizontal-vertical print difference due to mask shadowing and through-focus pattern placement errors that vary dramatically with pattern pitch.[1-3] If multiple patterning 193-nm immersion lithography at the 7 nm and lower technology nodes is to be replaced with single-exposure EUV lithography, then EUV projection optics with higher than 0.33 NA, more extreme off-axis illumination schemes, and/or masks with smaller 3D effects will be needed. In this paper, the performance of masks with Ru/Si ML reflective coatings[4,5] instead of the commonly used Mo/Si ML reflector is discussed. In Section 2.1, the current performance and some of the potential advantages of Ru/Si ML reflective coatings are summarized. In Section 2.2, recent improvements in Ru/Si ML performance with $B_4C$ interlayers are described. In Section 2.3, a model of a Ru/Si ML with $B_4C$ interlayers that can be used to accurately simulate the imaging performance of Ru/Si ML coatings in EUV scanners at 0.33 and 0.55 NA is presented. In Section 3, the results of rigorous simulations of various lithography performance parameters and the magnitude of mask 3D effects such as mask shadowing and telecentricity errors are presented. In Section 4 the main findings of the paper are summarized and some suggestions for future work are provided.

## 2. Ruthenium-Silicon Multilayer Reflective Coatings

### 2.1 Current State of Ru/Si ML Coatings

EUV reflectivity versus wavelength and EUV reflectivity versus angle of incidence for ideal Mo/Si and Ru/Si multilayers (no intermixing at the interfaces) using optical constants for Mo, Ru, and Si from the CXRO website[6] are shown in Fig. 1.

Due to the lower index of refraction of Ru compared to Mo, the spectral bandwidth of Ru/Si MLs is predicted to be significantly broader than that of Mo/Si MLs. The Ru/Si ML design saturates at a lower reflectivity than its Mo/Si counterpart because of the higher extinction coefficient of Ru compared to Mo. For this reason Ru/Si ML coatings have not normally been used on the reflective optics in EUV exposure tools. The higher extinction coefficient of Ru compared to Mo also causes the Ru/Si ML design to saturate with a smaller number of bilayers (~ 33) than its Mo/Si ML counterpart (~ 40) as shown in Fig. 2 (left) and, hence, Ru/Si ML coatings should potentially have lower defectivity.

Because of the lower index of refraction of Ru compared to Mo, the phase change upon reflection in Ru/Si exhibits a shallower gradient causing the effective reflectance plane in Ru/Si ML coatings to be ~10-15 nm closer to the coating surface, as shown in Fig. 2 (right). The results presented in this paper suggest that the use of Ru/Si ML coatings on EUV masks could lead to smaller mask 3D effects, i.e., less mask shadowing and smaller pattern placement (telecentricity) errors. Plots of EUV reflectivity versus wavelength at 6° angle of incidence and EUV reflectivity versus incident angle at 13.5 nm wavelength for ideal and state-of-the-art Ru/Si MLs with 20 bilayers are shown in Figure 3.

The comparisons of the reflectivity performance of ideal and state-of-the-art Ru/Si MLs shown in Figure 3 suggests that considerable improvements in the peak EUV reflectivity and the reflective bandwidth of Ru/Si MLs should be possible by employing interface engineering with C[7] or $B_4C$[8,9] interlayers to sharpen the interfaces.

### 2. Improvements in Ru/Si ML Coatings with $B_4C$ Interlayers

Just as is the case with the Mo/Si ML coatings that are present on the majority of all EUV reflective optics today, the width and roughness of the Ru-Si ML interfaces play a large role in determining the performance of Ru/Si ML coatings.[8] In this work, information on Ru-Si interfaces was obtained by depositing Ru/Si ML coatings with a variety of different coating designs on silicon wafers and measuring reflectivity versus wavelength and reflectivity versus angle of incidence in the EUV spectral region, collecting XTEM images of the films, and by matching simulation to experimental data. All of the Ru/Si ML coatings used in this work were deposited in low pressure Ar gas using a PVD tool. The Ru/Si test samples had different values for the total bilayer thickness, gamma values of 0.4 (where gamma is the fraction of the bilayer occupied by Ru), and with a variety of $B_4C$-interlayer thicknesses from 0 – 20 Å to retard interlayer diffusion and improve the Ru/Si interfaces. All of the Ru/Si coatings were designed to have a Si layer at the bottom of the film and a Ru layer at the top of the film, to have a multilayer period of ~7 nm to provide a maximum reflectivity at 13.5 nm wavelength at 6 degrees incident angle, and to have a total of 20 bilayers.

X-ray reflectometry (XRR) was used to determine the Ru/Si bilayer period of the coatings on the test samples.[10] An example of an XRR spectrum recorded from a Ru/Si ML-coated sample with 20 bilayers is shown in Figure 4 (left). A plot of *Slope* determined from

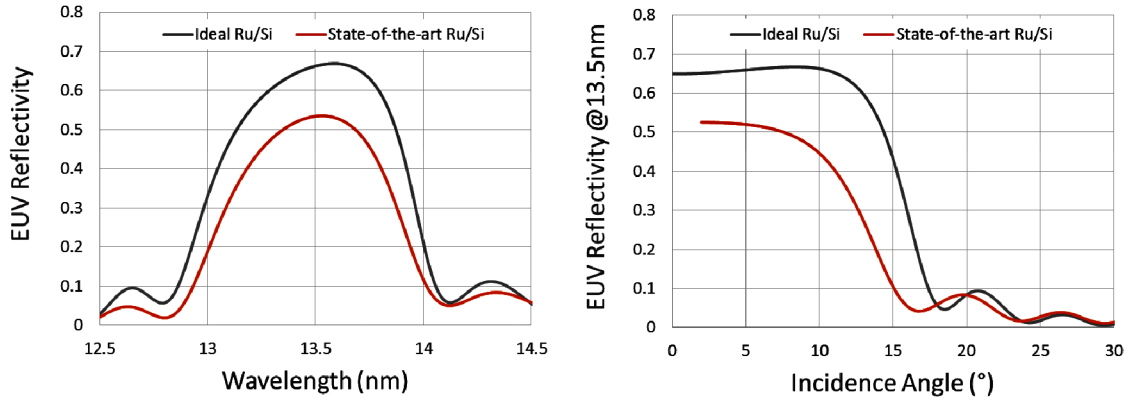


*Figure 3. Left: Plots of EUV reflectivity versus wavelength at 6° angle of incidence for ideal (grey) and state-of-the-art Ru/Si MLs with 20 bilayers (red). Right: Plots of EUV reflectivity versus incident angle at 13.5 nm wavelength for ideal (grey) and state-of-the- art Ru/Si MLs with 20 bilayers (red).*

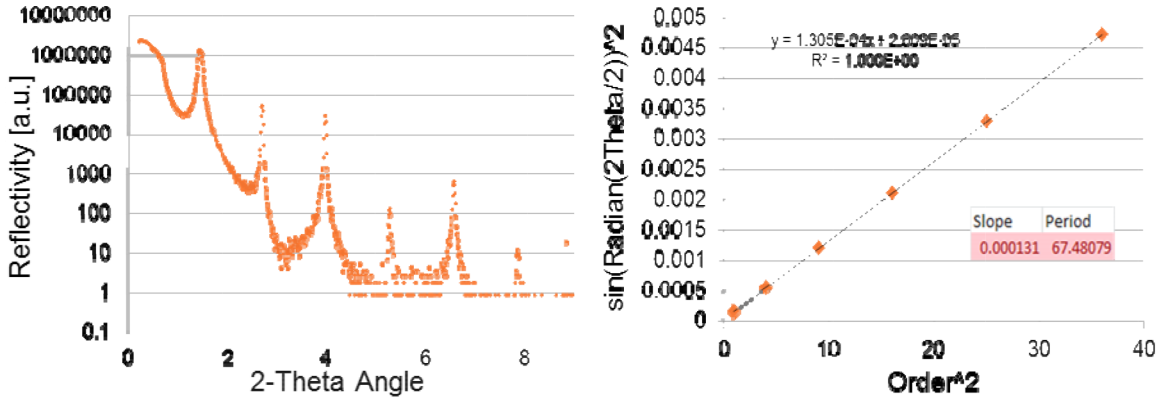


*Figure 4. Left: Plot of x-ray reflectivity (XRR) at 1.54060 Å wavelength versus 2-Theta Angle from a silicon wafer coated with 20 bilayers of Ru and Si. Right: X-ray reflectivity data plotted as* sin(Radian(2Theta/2))^2 *versus* Order^2 *which can be used in Equation 1 to accurately determine the ML Period.*

a plot of *sin(Radian(2Theta/2))^2* versus *Order^2* from the XRR data shown in Figure 4 (left) is shown in Figure 4 (right). The value of *Slope* can be used in Equation 1 to determine the ML period with sub-Å accuracy because of the extensive averaging involved.

$$\text{ML Period} = \frac{\lambda/2}{\sqrt{Slope}} \quad \text{where } \lambda = 1.54060 \text{ Å} \qquad (1)$$

More than 20 Si wafers were coated with Ru/Si ML films with $B_4C$ interlayers at various thickness from 0 to 20 Å. For these samples ML Period Contraction values were determined from Equation 2 using the known thickness of Ru, $B_4C$ and Si deposited layers and the XRR-measured ML Period values.

$$\text{ML Period Contraction} = \text{ML Period (Measured)} + T_{Ru} + T_{B4C} + T_{Si} \qquad (2)$$

If no $B_4C$ interlayers were present and no interdiffusion of the Ru and Si layers took place or no compounds (silicides) were formed then there would be no significant period contraction. In such cases the interfaces between Ru and Si would be narrow and the synthetic Bragg reflectivity of the resulting film would be expected to be high. In films in which $B_4C$ interlayers were present, the $B_4C$ thickness values that resulted in the lowest values of ML Period Contraction were found to correspond to coatings with the highest peak EUV reflectivity and widest EUV reflective bandwidth. Then, according to the data plotted in Figure 5, the optimum $B_4C$ interlayer films should be approximately 10 Å thick for both interfaces, i.e., on top of Si and on top of Ru.

Measurements of reflectivity versus EUV wavelength and EUV reflectivity versus angle of incidence of a Ru/Si ML coating with 20 bilayers with and without 10 Å thick $B_4C$ interlayers at both types of Ru-Si interfaces were carried out using the EUV Standards and Calibration beamline at the Advanced Light Source in Berkeley. Figure 6 shows that the peak reflectivity and reflective bandwidth of the Ru/Si ML with $B_4C$ interlayers have clearly been improved but coating performance is still dominated by interdiffusion.

### 2.3 Development of Ru/Si ML with $B_4C$ Interlayer Model

Electron energy loss spectra (EELS) collected from a sample of Ru/Si ML with 10 Å thick $B_4C$ interfaces deposited on both types of Ru-Si interfaces are shown in Figure 7. Five distinct layers can be identified within each Ru-Si period and the atomic percentage of the constituent elements is given in the table of Figure 7.

Figure 8 compares for a 20 bilayer Ru/Si coated sample with 10 Å thick $B_4C$ interlayers at each type of interface the measured reflectivity versus wavelength and reflectivity at 13.5 nm wavelength versus angle of incidence (solid line) to the simulated curves (dashed) obtained with a model based on the input parameters listed in Table 1.

The measured reflectivity versus wavelength data shown in Figure 8 were fitted at the 5 wavelengths indicated with arrows with S-Litho EUV (Synopsys)[11] using the thickness values and atomic ratios determined from the EELS spectra shown in Figure 7 and by allowing the thickness of the top-most layers and the

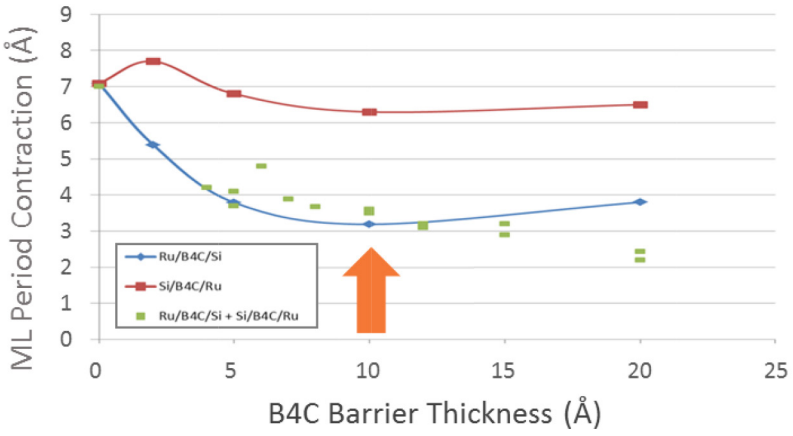


*Figure 5. Plot of ML Period Contraction versus $B_4C$ barrier thickness for both types of Ru-Si interfaces, i.e., with $B_4C$ films deposited on top of the Si layers and with $B_4C$ layers deposited on top of the Ru layers showing that the optimum $B_4C$ barrier thicknesses in both cases are approximately 10 Å.*

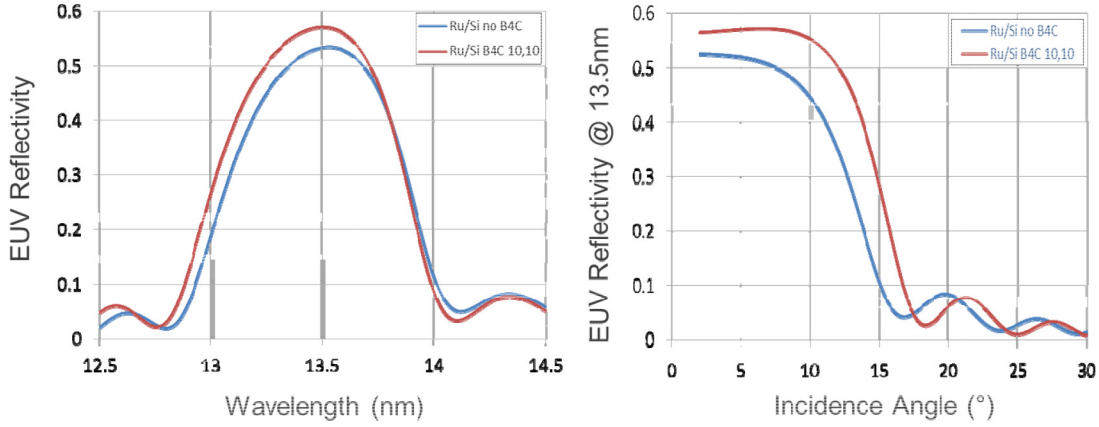


*Figure 6. Plots of measured EUV reflectivity versus wavelength and EUV reflectivity at 13.5 nm wavelength versus angle of incidence of a 20 bilayers Ru/Si ML coated sample with and without 10 Å thick $B_4C$ interlayers.*

densities of the 5 distinct layers in each Ru/Si bilayer period to vary. The fitted densities of the compounds were constrained be less than those of the pure materials. The optimum density values and optical constants determined as a result of the S-Litho fitting are listed in Table 1 (on the right).

Figure 8 shows that reasonable agreement between measurement and simulation has been obtained with the 5-layer model for each Ru-Si bilayer period. Especially the achieved correspondence for the angular reflectivity at 13.5nm wavelength is a strong validation of the obtained Ru/Si ML model.

## 3. Results of Rigorous Simulations

To better understand the impact of the new broader bandwidth Ru/Si ML reflector on mask 3D effects, we looked into the imaging simulations at 0.33 NA and 4x magnification and at 0.55 NA and anamorphic 4x/8x magnification[12] with both Quasar ($\sigma_o$ 0.9/$\sigma_i$ 0.4/ deg45) and Dipole Y ($\sigma_o$ 0.9/$\sigma_i$ 0.35/ deg90) illumination. The simulation results described in this paper were performed using the rigorous mask 3D simulator S-Litho EUV (Synopsys)[11] using a calibrated and verified mask model for standard Mo/Si ML mirror with 40 bilayers including Mo-Si intermixing[13] and for an ideal (no Ru-Si intermixing) Ru/Si ML mirror with 20 bilayers using the optical constants (n & k values at 13.5 nm wavelength) and for the modeled Ru/Si ML mirror with optimum $B_4C$ interlayers described in Section 2.2, all with a patterned 70 nm thick Ta-based absorber. The components for the three different mask stack models are summarized in Table 2.

### 3.1 Rigorous Simulation Results at 0.33 NA and 4x magnification

Simulation results for the horizontal-vertical bias of a 16 nm CD trench through LS pitch at 0.33 NA and 4x magnification with Quasar illumination for the 3 different mask stacks listed in Table 2 is shown in Fig. 9. Simulation results for telecentricity error through LS pitch at 0.33 NA and 4x magnification with Dipole Y illumination for the 3 different mask stacks listed in Table 2 are also shown in Fig. 9.

The data in Figure 9 show that the Ru/Si ML reflector significantly reduces shadow bias and exhibits less pattern shift through focus than a standard Mo/Si ML mirror. The modeled Ru/Si ML with $B_4C$ interlayers shows similar benefits to the ideal Ru/Si ML, indicating that the shallower plane of reflection of Ru/Si ML coatings is responsible for the reduced mask 3D effects.

Simulation of the aerial image through focus and the process windows for the printing of a horizontal two-bar trench pattern (18 nm CD, 36 nm pitch, and 250 nm length) at 0.33 NA (4x magnification) and 6° chief-ray-angle for a Mo/Si ML and for a Ru/Si ML

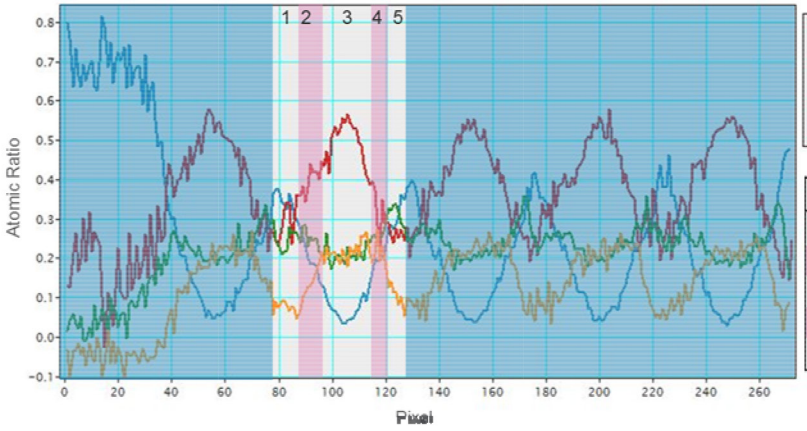


| Layer No | Si | B | C | Ru |
|---|---|---|---|---|
| 1 | 40% | 30% | 25% | 5% |
| 2 | 23% | 43% | 23% | 13% |
| 3 | 5% | 55% | 20% | 20% |
| 4 | 20% | 40% | 28% | 13% |
| 5 | 35% | 25% | 35% | 5% |

*Figure 7. Left: Plots of EELS profiles for Silicon, Boron, Carbon and Ruthenium from a silicon wafer coated with a Ru/Si ML with 10 Å thick $B_4C$ interlayers as a function of film height (the Si wafer is located at the left). Right: Table listing the percentage of Si, B, C and Ru present in each of the 5 distinct layers that can be identified within each Ru-Si period.*

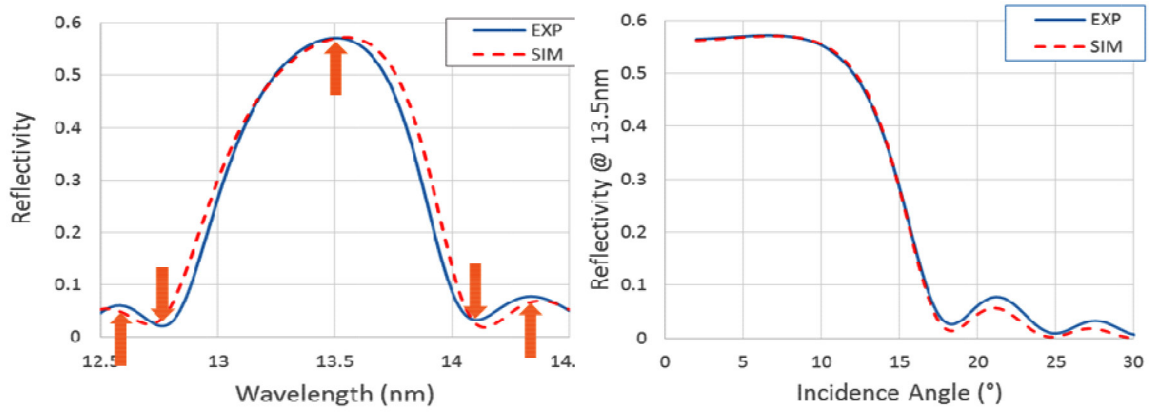


*Figure 8. Comparison of measured (solid line) and simulated (dashed line) reflectivity versus wavelength (left) and reflectivity at 13.5 nm wavelength versus incident angle (right) showing that reasonable agreement between measured and simulated EUV reflectivity can be obtained with a 5 layer model for each Ru/Si period.*

with $B_4C$ interlayers is shown in Figure 10.

The aerial images through focus in Figure 10 show that improved symmetry through focus between the two trenches of the 2 bar pattern can be achieved with a Ru/Si ML with $B_4C$ interlayer (bottom) than with a Mo/Si ML coating (top), resulting in a wider overlapping process window.

### 3.2 Rigorous Simulation Results at 0.55 NA and anamorphic 4x/8x magnification

Simulation results at 0.55 NA and anamorphic 4x/8x magnification for the horizontal-vertical bias of 10 nm CD trench through LS pitch with Quasar illumination for the 3 different mask stack listed in Table 2 are shown in Figure 11, as well as for telecentricity error though LS pitch with Dipole-Y illumination.

Going from NA0.33 at 4x magnification to NA0.55 at 8x magnification decreases the angular capture range on mask. The related ML reflectivity apodization (cf. Fig. 1) is more reduced for the standard Mo/Si ML than for the Ru/Si ML. This causes the H-V bias versus pitch behavior at 0.55 NA and anamorphic 4x/8x magnification to be similar for Mo/Si and Ru/Si MLs.

However, the benefit of the Ru/Si ML mirror at NA0.55 and anamorphic 4x/8x magnification is still visible in the pattern shift through focus (telecentricity error) performance through pitch shown in Figure 11, where the performance of ideal Ru/Si MLs is better than that of modeled Ru/Si MLs is better than that of Mo/Si MLs.

Simulated aerial image through focus of a horizontal two-bar trench pattern (12 nm CD, 22 nm pitch, and 250 nm length) at 0.55 NA and anamorphic 4x/8x magnification for a mask with a Mo/Si ML mirror and with a Ru/Si ML mirror with $B_4C$ interlayers is shown in Figure 12, as well as the corresponding process windows.

The data plotted in Figure 12 show improved symmetry through focus and more overlap in the process windows of the trenches of the 2 Bar pattern when imaging with Ru/Si ML coatings with $B_4C$ interlayers than with standard Mo/Si ML coatings.

## 4. Conclusions & Suggestions for Future Work

Non-telecentric illumination of the reflective mask in an EUV lithography tool leads to a variety of mask 3D effects including horizontal-vertical print differences and through-focus pattern placement (telecentricity) errors on the printed wafer. In this paper, we have shown that Ru/Si ML reflective coatings may be a viable alternative to the Mo/Si ML coatings that are in common use to-

**Table 1. Table of input parameters for a model of a Ru/Si ML coating with 20 bilayers and with 10 Å thick $B_4C$ barrier layers on the top of each internal Ru and Si layer with layer thicknesses and atomic compositions determined from the elemental EELS profiles shown in Figure 7 and with thickness of the top-most layers and the densities of the 5 distinct layers within each bilayer period determined with SLitho simulation software by fitting to the reflectivity data shown in Figure 8.**

| Layer | Compound | Period Thickness [Å] | Top Thickness [Å] | Density [g/cm³] | n @ 13.5nm | k @ 13.5nm |
|---|---|---|---|---|---|---|
| 3 | Si1_B11_C4_Ru4 | | 61 | | | |
| **2** | **Si9_B17_C9_Ru5** | | **4.1** | | | |
| 1 | Si8_B6_C5_Ru1 | | 3.4 | | | |
| **5** | **SI7_B5_C7_Ru1** | **9.9** | | **0.66** | **0.995** | **-0.001** |
| 4 | Si8_B16_C11_Ru5 | 8.6 | | 2.66 | 0.976 | -0.004 |
| **3** | **Si1_B11_C4_Ru4** | **23.9** | | **11** | **0.887** | **-0.017** |
| 2 | Si9_B17_C9_Ru5 | 15.8 | | 0.66 | 0.994 | -0.001 |
| **1** | **Si8_B6_C5_Ru1** | **12.2** | | **0.66** | **0.996** | **-0.001** |
| | **Period** | **70.3** | | | | |

**Table 2. Compilation of the mask stack models used for the simulations.**

| Stack No. | Multilayer | Absorber |
|---|---|---|
| MoSi ML | 40 bilayer Mo/Si with intermixing | 70 nm thick Ta-based |
| Ideal RuSi ML | 20 bilayer Ru/Si no intermixing | 70 nm thick Ta-based |
| RuSi ML w/ B4C | 20 bilayer Ru/Si w/ B4C barriers | 70 nm thick Ta-based |

day because the lower index of refraction of Ru compared to Mo causes the effective reflective plane in Ru/Si ML coatings to be closer to the ML surface resulting in less severe mask 3D effects. We have shown that the peak reflectivity and reflective bandwidth of state-of-the-art Ru/Si ML coatings can be significantly improved by adding $B_4C$ interlayers to reduce Ru-Si interdiffusion and improve the coating performance, but the overall performance of the Ru/Si ML coatings is still inferior to the predicted performance of ideal Ru/Si ML coatings. In conclusion, we have used rigorous simulations to show that mask stacks comprised of the broader bandwidth Ru/Si ML reflector will significantly reduce mask 3D effect on wafer imaging because the reduced intensity apodization and shallower plane of reflection leads to significantly smaller mask shadow effects, smaller pattern shifts through focus and smaller CD asymmetry and wider process window when printing horizontal 2-bar patterns with current 0.33 NA (4x magnification) EUV exposure tools and with future 0.55 NA (anamorphic 4x/8x magnification) EUV exposure tools. In combination with an optimized mask absorber the mask 3D effects can be further reduced.[7,14] Future work will include the evaluation of the printing performance of an EUV mask with a Ru/Si ML reflective coating in a 0.33 NA EUV scanner.

## 5. Acknowledgements

The authors would like to thank Mandeep Singh of Newport Corporation for pointing out to us the advantages of Ru/Si multilayer coatings. The authors would also like to thank Scott Zaffini of JX Nippon Mining & Metals for supplying the targets needed to fabricate the ML samples. Lastly, we gratefully acknowledge the encouragement and support of Eric Hendrickx of IMEC and Professor Marc Heyns of KU Leuven.

## 6. References

[1] Philipsen, V., Hendrickx, E., Jonckheere, R., Vandenberghe, G., Davydova, N., Fliervoet, T., Neumann, J.T., "Impact of mask stack on high NA EUV imaging," International Symposium on Extreme Ultraviolet Lithography, Brussels, Belgium (2012).

[2] Neumann, J.T., Graupner, P., Kaiser, W., Garreis, R., Geh, B., "Interaction of 3D mask effects and NA in EUV lithography," **Proc. SPIE 8522,** 852211 (2012).

[3] Philipsen, V., Mochi I., Van Look L., Lorusso G., Luong K.V., Hendrickx E., Wittebrood F., Schiffelers G., van Setten E., Fliervoet, T., Dusa M., "NXE:3300 insertion for N7 : status and challenges," International Symposium on Extreme Ultraviolet Lithography, Maastricht, Netherlands (2015).

[4] Stearns, D., Rosen, R., Vernon, S., "High-performance multilayer mirrors for soft x-ray projection lithography," **Proc. SPIE 1547,** 2 (1992).

[5] Windt, D., Hall, R., Waskiewicz, W., "Interface imperfections in metal/Si multilayers," *J. Appl. Phys. 71,* 2675 (1992).

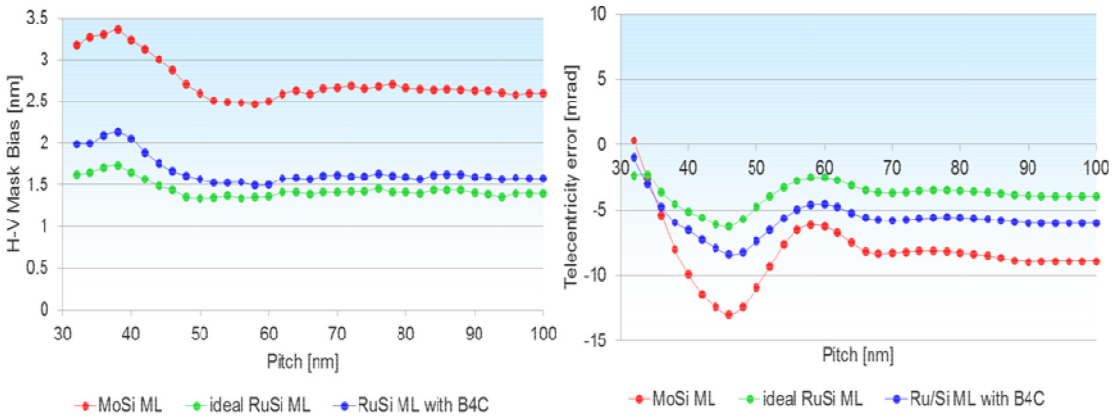


*Figure 9. Left: Simulation of horizontal-vertical bias for CD 16 nm trench through L/S pitch at 0.33 NA (4x magnification) and 6° chief-ray-angle with Quasar illumination for the 3 different mask stacks listed in Table 2. Right: Simulation of telecentricity error for CD 16 nm trench through L/S pitch at 0.33 NA (4x magnification) and 6° chief-ray-angle with Dipole Y illumination for the 3 different mask stacks listed in Table 2.*

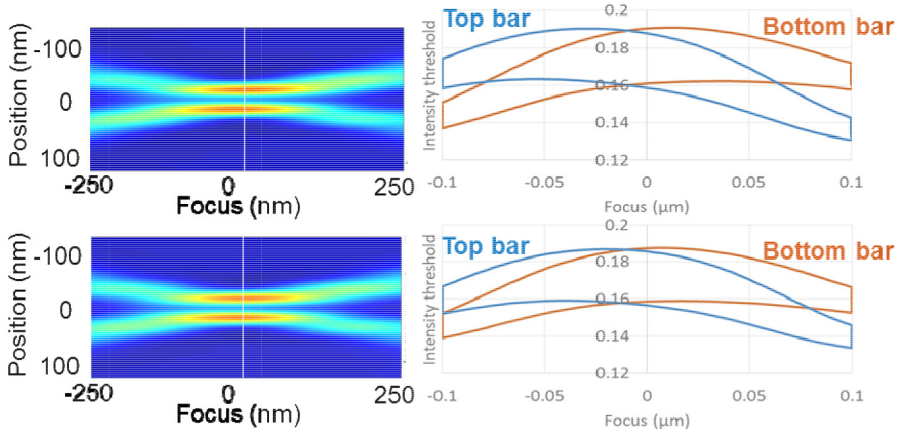


*Figure 10. Simulation of aerial image through focus and Process Windows of a horizontal two-bar trench pattern (18 nm CD, 36 nm pitch, and 250 nm length) at 0.33 NA (4x magnification) and 6° chief-ray-angle with Dipole-Y illumination on a mask with a Mo/Si ML coating (top) and a Ru/Si ML coating with $B_4C$ interlayers (bottom).*


[6] CXRO X-ray database, http://henke.lbl.gov/optical-constants/

[7] Wood, O., Raghunathan, S., Mangat, P., Philipsen, V., Luong, V., Kearney, P., Verduijn, E., Kumar, A., Patil, S., Laubis, C., Soltwisch, V., Scholze, F., "Alternative materials for high numerical aperture extreme ultraviolet lithography mask stacks," **Proc. SPIE 9422,** 94220I (2015).

[8] Bajt, S., Alameda, J., Barbee Jr, T., Clift, M., Folta, J., Kauffman, B., Spiller, E., "Improved reflectance and stability of Mo/Si mirrors," **Proc. SPIE 4506,** 65 (2001).

[9] Bruijn, S., v.d. Kruijs, R., Yakshin, A., Zoethout, E., Bijkerk, F., "Thermally induced decomposition of $B_4C$ barrier layers in Mo/Si multilayer structures," *Surface & Coating Technology 205,* 2469 (2010).

[10] Yakshin, A., Louis, E., Gorts, P., Maas, E., Bijkerk, F., "Determination of the layered structure in Mo/Si multilayers by grazing incidence x-ray reflectometry," *Physica B 293,* 141 (2000).

[11] http://www.synopsys.com/Tools/Manufacturing/MaskSynthesis/Pages/Sentaurus-Lithography.aspx.

[12] Migura, S., Kneer, B., Neumann, J. T., Kaiser, W., van Schoot, J., "EUV lithography optics for sub 9 nm resolution," Oral presentation at the International Symposium on Extreme Ultraviolet Lithography, Washington, D.C., Oct. 29, 2014.

[13] Philipsen, V., Hendrickx, E., Jonckheere, R., Davydova, N., Fliervoet, T., Neumann, J. T., "Actinic characterization and modeling of the EUV mask stack," **Proc. SPIE 8886,** 888619 (2013).

[14] Luong K.V., Philipsen, V., Hendrickx E., Verduijn, E., Wood, O., Scholze, F., "Modeling EUV mask using alternative materials for Mask3D effect compensation," International Symposium on Extreme Ultraviolet Lithography, Maastricht, Netherlands (2015).

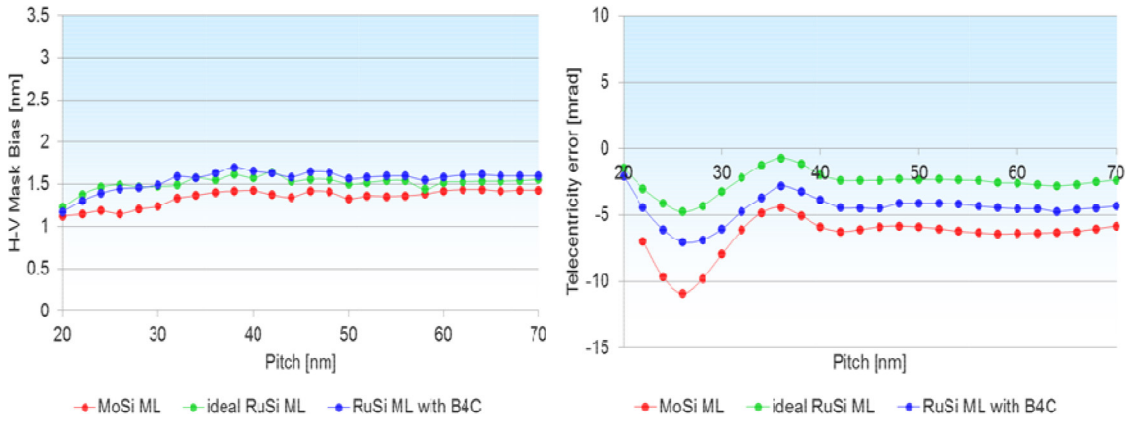


*Figure 11. Left: Simulation of horizontal-vertical bias for a 10 nm CD trench through LS pitch at 0.55 NA (anamorphic 4x/8x magnification) with Quasar il umination for the 3 different mask stacks given in Table 2. Right: Simulation of telecentricity error for 10 nm CD trench through LS pitch at 0.55 NA (anamorphic 4x/8x magnification) with Dipole Y illumination for the 3 different mask stacks given in Table 2.*

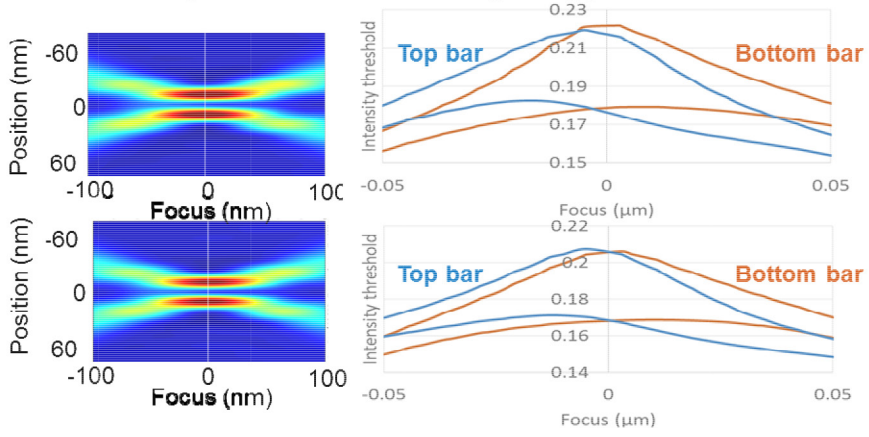


*Figure 12. Simulation of aerial image through focus (left) and Process Windows (right) of a horizontal two-bar trench pattern (12 nm CD, 22 nm pitch, and 250 nm length) at 0.55 NA (anamorphic 4x/8x magnification) with Dipole-Y illumination on a mask with a Mo/Si ML coating (top) and a Ru/Si ML coating with $B_4C$ interlayers (bottom).*

## No Rest for the Mask Industry

*(continued from page 2*

structures. Such technologies may have been held back due to the increased shot counts associated with the number of polygons required to generate complex OPC shapes, driving increased write times/mask manufacturing cycle times with today's existing e-Beam writing technologies. Improvements in pattern placement accuracy should also help enable the extension of 193 nm immersion to multiple patterning processes, including self-aligned quadruple and maybe even octuple sidewall patterning and tighter cut mask layers.

While the OPC convergence times may remain a challenge for OPC teams and the data volumes will increase significantly, there are solutions in the marketplace to support the remaining mask infrastructure including defect disposition and inspection technologies. The role of mask proximity correction (MPC) in delivering the correct final dimensions at wafer level has also been the subject of extensive research, and software solutions to deliver MPC of the same quality as OPC are rapidly becoming available.

In summary, while the pitch and linewidth of the main patterns on masks may no longer be shrinking at the same rate as in the past, new requirements on process control, including CD, registration and EPE, as well as tighter control of defect levels and the entire enabling infrastructure for EUV adoption will continue to present us with many challenging issues for years to come. In the coming years we should expect to see exciting new advancements and innovative technical papers presented at industry symposia.

BACUS N • E • W • S

## Sponsorship Opportunities

**Sign up now for the best sponsorship opportunities**

**Advanced Lithography 2017 —**
**Contact:** Teresa Roles-Meier,
Tel: +1 360 685 5445; **teresar@spie.org**

**Photomask 2016 —**
**Contact:** Melissa Farlow,
Tel: +1 360 685 5596; **melissaf@spie.org**

## Advertise in the BACUS News!

**The BACUS Newsletter is the premier publication serving the photomask industry. For information on how to advertise, contact:**

Melissa Farlow,
Tel: +1 360 685 5596
**melissaf@spie.org**

## BACUS Corporate Members

Acuphase Inc.
American Coating Technologies LLC
AMETEK Precitech, Inc.
Berliner Glas KGaA Herbert Kubatz GmbH & Co.
FUJIFILM Electronic Materials U.S.A., Inc.
Gudeng Precision Industrial Co., Ltd.
Halocarbon Products
HamaTech APE GmbH & Co. KG
Hitachi High Technologies America, Inc.
JEOL USA Inc.
Mentor Graphics Corp.
Molecular Imprints, Inc.
Panavision Federal Systems, LLC
Profilocolore Srl
Raytheon ELCAN Optical Technologies
XYALIS

# Industry Briefs

## Next EUV Challenge: Pellicles

**Mark Lapedus,** Semiconductor Engineering

April 27, 2016 — Both the EUV light source and resists are making noticeable progress. And then, there is the EUV mask infrastructure, which has gaps. Challenges remain with pellicles at the full power of the light source and with actinic inspection. ASML, the sole supplier of EUV pellicles in the industry, is still in the prototype and/or pilot line stage with this technology. ASML's EUV pellicles for production are expected to ship by mid-2017. But it's unclear if EUV pellicles will be ready in time. ASML's polysilicon-based EUV pellicle, which is just 50nm thick, must withstand an enormous amount of heat. In theory, the pellicle will dissipate the heat. But at those temperatures, there are also fears that the EUV pellicle could deteriorate or break during processing.

An EUV pellicle must meet various requirements in three basic categories-transmission rates; thermal loads; and productivity. The industry wants an EUV pellicle with a transmission rate of 90% (single pass) and 81% (double pass). So far, though, the initial polysilicon-based EUV pellicles from ASML have transmission of about 85% (single pass), which is still short of the industry's target. ASML will likely solve this problem in the near term. In 2016, ASML is expected to upgrade the power source for its EUV scanners from 80 watts to 125 watts developing EUV pellicles with a new heat dissipation layer. Initially, the industry will use ASML's polysilicon membrane. A pellicle with 90% transmission rates for 250-watt sources is expected to ship by mid-2017. There is a catch, however. Mask makers can't use existing 193nm mask inspection tools to directly inspect EUV masks with a polysilicon-based pellicle. This material is opaque at the deep ultraviolet range. Seeking to solve the problem, ASML has developed a retractable pellicle. In a theoretical flow, the EUV mask is manufactured and the pellicle is placed on top. In the inspection process, the EUV pellicle is automatically raised and removed from the mask. Then, once the inspection process is finished, the pellicle is automatically lowered and re-attached. Still, there is a chance that a retractable pellicle may experience a glitch in the flow. So long term, the industry wants an actinic-based mask inspection tool, which can inspect a mask without removing the pellicle. But it could take the industry three to five more years at a cost of around $500 million. And so far, no fab tool vendor has committed the resources to develop such a tool.

## 7 nm Fab Challenges

**Mark Lapedus,** Semiconductor Engineering

April 21, 2016 — At 7 nm, chipmakers hope to use two types of techniques in a complementary fashion: EUV and immersion/multi-patterning. Today, though, the status of EUV is uncertain. So initially, chipmakers plan to use 193 nm immersion/multi-patterning. Then, if it's ready, EUV will be inserted later for some layers. If it's not ready, EUV will slip to 5 nm. OPC makes use of assist features, which are getting smaller and more complex at each node. In addition, the number of masks per mask set is increasing at each node. At 16 nm, for example, there are 60 masks. This figure is expected to jump to 77 at less than 11 nm. Each of the mask patterns is also getting more complex because each feature needs to be written more precisely. More aggressive OPC, like ILT (inverse lithography) or shapes approaching ILT shapes, are needed to get the required process window. As a result, it will take a longer time to write or pattern the mask using today's e-beam mask writers. This, in turn, equates to longer mask turnaround times and higher costs. Meanwhile, if the industry inserts EUV at 7 nm, mask makers must contend with the complexities of EUV masks. For EUV, the sub-resolution assist feature (SRAF) sizes range from 32 nm to 40 nm, compared to 60 nm for optical. All told, the write times for EUV masks are long. To reduce the write times, photomask makers want a new class of multi-beam mask writers. Still to be seen, however, is if these tools will be ready in time for 7 nm.

## EUV Production Insertion

**www.asml.com**

April 14, 2016 — The consensus emerging from the 2016 SPIE Advanced Lithography conference was that we're close, but not quite there yet. ASML expects the first IC manufacturers to start using EUV for chip production from 2018. With the lead time to get systems built, installed in fabs and qualified for production, this means 2016 is the year when the in-principle decision to insert EUV in 2018 will have to be made. A productivity of around 1,500 wafers per day makes EUV more cost-effective than multiple patterning. When taking into account the additional benefits of EUV, such as better yield and faster time to market, the cost cross-over point may even be substantially lower.

ASML's 2016 productivity target is to achieve the 1,500 wafer-per-day milestone. The 2016 target for availability is 80 percent, but it is clear that availability needs to continue to improve further, towards the levels that are achieved by immersion systems today (above 95 percent). On both fronts, ASML is on track. Multiple EUV systems, both at ASML and at customer sites, have demonstrated the capability to process more than 1,000 wafers per day. ASML's latest EUV system, the NXE:3350B, has shown a peak productivity of 1,368 wafers in a 24-hour period.

# Join the premier professional organization for mask makers and mask users!

## About the BACUS Group

Founded in 1980 by a group of chrome blank users wanting a single voice to interact with suppliers, BACUS has grown to become the largest and most widely known forum for the exchange of technical information of interest to photomask and reticle makers. BACUS joined SPIE in January of 1991 to expand the exchange of information with mask makers around the world.

The group sponsors an informative monthly meeting and newsletter, BACUS News. The BACUS annual Photomask Technology Symposium covers photomask technology, photomask processes, lithography, materials and resists, phase shift masks, inspection and repair, metrology, and quality and manufacturing management.

### Individual Membership Benefits include:

- Subscription to BACUS News (monthly)
- Eligibility to hold office on BACUS Steering Committee

www.spie.org/bacushome

### Corporate Membership Benefits include:

- 3-10 Voting Members in the SPIE General Membership, depending on tier level
- Subscription to BACUS News (monthly)
- One online SPIE Journal Subscription
- Listed as a Corporate Member in the BACUS Monthly Newsletter

www.spie.org/bacushome

## Calendar

**2016**

**SPIE Photomask Technology**
12-14 September 2016
**San Jose Convention Center**
San Jose, California, USA
**www.spie.org/pm**

**2017**

**SPIE Advanced Lithography**
26 February-2 March 2017
San Jose Marriott and
San Jose Convention Center
San Jose, California, USA
**www.spie.org/al**

SPIE is the international society for optics and photonics, an educational not-for-profit organization founded in 1955 to advance light-based science and technology. The Society serves nearly 264,000 constituents from approximately 166 countries, offering conferences and their published proceedings, continuing education, books, journals, and the SPIE Digital Library in support of interdisciplinary information exchange, professional networking, and patent precedent. SPIE provided more than $5.2 million in support of education and outreach programs in 2015. **www.spie.org**

**SPIE.**
*International Headquarters*
P.O. Box 10, Bellingham, WA 98227-0010 USA
Tel: +1 360 676 3290
Fax: +1 360 647 1445
help@spie.org • **www.SPIE.org**

*Shipping Address*
1000 20th St., Bellingham, WA 98225-6705 USA

**Managed by SPIE Europe**
2 Alexandra Gate, Ffordd Pengam, Cardiff,
CF24 2SA, UK
Tel: +44 29 2089 4747
Fax: +44 29 2089 4750
spieeurope@spieeurope.org • **www.spieeurope.org**

You are invited to submit events of interest for this calendar. Please send to lindad@spie.org; alternatively, email or fax to SPIE.